Palaeogeography, Palaeoclimatology, Palaeoecology 510 (2018) 49–62

Contents lists available at ScienceDirect

Palaeogeography, Palaeoclimatology, Palaeoecology

journal homepage: www.elsevier.com/locate/palaeo

Geochemical and detrital zircon U-Pb geochronological constraints on provenance of the Xiaomei red earth sediments (Bose Basin, Guangxi Province, southern China)

Feng Cheng[a], Hanlie Hong[a,b,*], Christopher J. Bae[c,**], Zhaohui Li[d], Thomas J. Algeo[b,e,f], Shengmin Huang[a,g], Liuling Cheng[a], Qian Fang[a]

[a] School of Earth Sciences, China University of Geosciences, Wuhan, Hubei 430074, China
[b] State Key Laboratory of Biogeology and Environmental Geology, China University of Geosciences, Wuhan, Hubei 430074, China
[c] Department of Anthropology, University of Hawaii at Manoa, 2424 Maile Way, 346 Saunders Hall, Honolulu, HI 96822, USA
[d] Department of Geosciences, University of Wisconsin, Parkside, Kenosha, WI 53144, USA
[e] Department of Geology, University of Cincinnati, Cincinnati, OH 45221-0013, USA
[f] State Key Laboratory of Geological Processes and Mineral Resources, China University of Geosciences, Wuhan, Hubei 430074, China
[g] Nanning Museum, Nanning, Guangxi Zhuang Autonomous Region 530012, China

ARTICLE INFO

Keywords:
Loess
Paleosol
Red earth sediments
Chemical weathering
U-Pb dating
Nd isotopes

ABSTRACT

The Bose Basin in southern China is within a region influenced by the winter westerly monsoon and, thus, potentially subject to eolian dust accumulation. A red earth sequence developed on terraces of the Youjiang River (a branch of the Pearl River) records information about climate variation during the Pleistocene and its relationship to contemporaneous global climate changes. In this study, geochemical characteristics and U-Pb geochronology of detrital zircons of the red earth sequence at Xiaomei were investigated using X-ray diffraction (XRD), X-ray fluorescence (XRF), inductively coupled plasma mass spectrometry (ICP-MS), thermal ionization mass spectrometry (TIMS), and detrital zircon U-Pb dating analyses. Our results show that the red earth sediments are composed of quartz and clay minerals (kaolinite, illite, and mixed-layer illite/vermiculite) with minor hematite and goethite. Mobile elements such as CaO, MgO, Na_2O, K_2O, Sr and Ba are depleted and immobile elements such as TiO_2, Al_2O_3, Fe_2O_3(t) and Zr are enriched in comparison with loess-paleosols of the Chinese Loess Plateau (CLP), the upper continental crust (UCC), and post-Archean Australian shale (PAAS). These data indicate that the Xiaomei red earth sediments have experienced intense chemical weathering, similar to that of the Xuancheng and Jiujiang red earth sections on the middle to lower reaches of the Yangtze River. The Xiaomei sediments have similar La/Th ratios, U/Pb vs. Th/Pb relationships, and rare earth element (REE) distributions to the CLP, UCC, and PAAS, and their low $\varepsilon_{Nd}(0)$ values are indicative of an upper crustal origin. The $^{147}Sm/^{144}Nd$ and $^{87}Sr/^{86}Sr$ ratios of the Xiaomei sediments are different from loess-paleosols of the CLP but similar to those of well-mixed river sediments. U-Pb dating of detrital zircons in the Xiaomei sediments shows that crystals from different units have slightly different age distributions. The full Xiaomei section yields a distribution similar to that of Upper Permian-Triassic clastic rocks in the Youjiang area, and the distribution of the middle to upper Xiaomei section additionally shows similarities to upper crust of the South China Craton. Our results indicate that the Xiaomei red earth sequence, which dates to the late Early to early Middle Pleistocene (~1.0–0.6 Ma), accumulated predominantly from fluvially transported, locally weathered materials and, therefore, that the sediment-carrying capacity of the East Asian winter monsoon has been overestimated in previous provenance studies of red earth sediments in South China.

1. Introduction

Formation of geologically young red earth sequences in southern China is considered to be related to a mid-Quaternary (~1.2–0.6 Ma) phase of uplift of the Tibetan Plateau known as the 'Kunhuang movement', which resulted in a rapid increase in elevation to close to its present level (Wang et al., 2009). This uplift has been linked to intensification of the Asian monsoons owing to enhanced land-sea

* Correspondence to: H. Hong, School of Earth Sciences, China University of Geosciences, Wuhan, Hubei 430074, China.
** Corresponding author.
E-mail addresses: honghl8311@aliyun.com (H. Hong), cjbae@hawaii.edu (C.J. Bae).

https://doi.org/10.1016/j.palaeo.2017.08.040
Received 13 January 2017; Received in revised form 2 August 2017; Accepted 24 August 2017
Available online 28 September 2017
0031-0182/ © 2017 Elsevier B.V. All rights reserved.

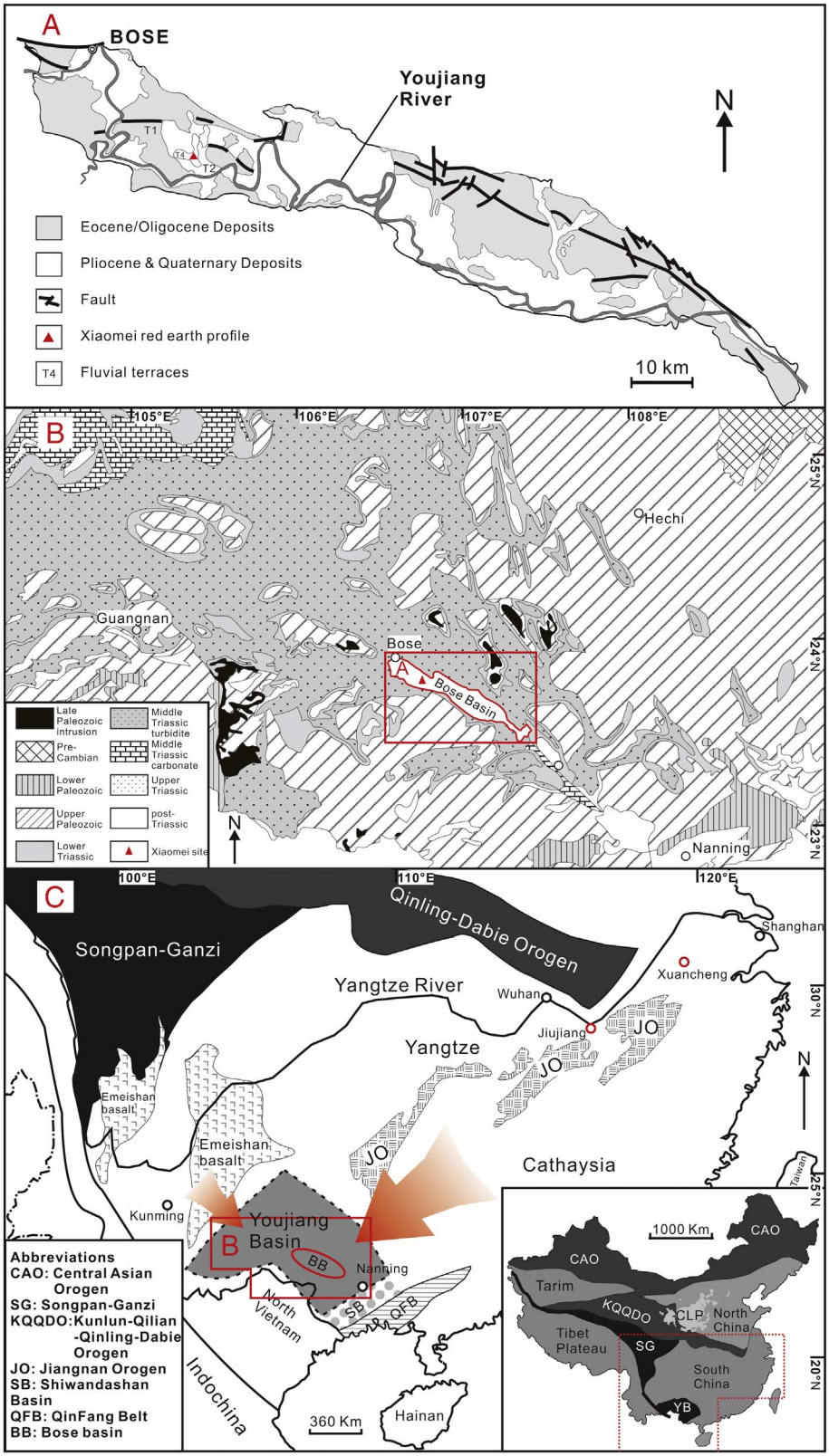

Fig. 1. Location of the study region on different map scales. (A) The magnified area as marked in figure B showing the site of the Xiaomei red earth profile (adapted from Hou et al., 2000); (B) geological map of Youjiang area showing the location of the study region and the stratigraphic distribution of potential detrital zircons for Xiaomei red earth deposits, Bose Basin (adapted from the 1:200,000 map of the Guangxi Zhuang Autonomous Region, Guizhou and Yunnan provinces); (C) general paleogeography and tectonic units of South China with the transportation path of clastic materials to Youjiang area during the Late Permian to Middle Triassic (adapted from Yang et al., 2012a and 1:12,000,000 tectonic map of China).

seasonal thermal contrasts (An, 2014). Among other effects, it has displaced the westerlies southward and caused aridification of the interior of Asia, triggering expansion of the Gobi Desert in northwestern China (Gallet et al., 1996). An increasing flux of eolian materials from the northern Tibetan Plateau, transported via monsoonal winds, has resulted in widespread accumulation of loess-paleosol deposits in East Asia during the Middle to Late Quaternary (Derbyshire et al., 1998; Bookhagen et al., 2005). These loess-paleosol sequences document regular climatic and environmental changes that conform to the oxygen isotope and other climate proxy records from deep-sea sediments and ice cores (Costantini et al., 2009; Sheldon and Tabor, 2009). On the Chinese Loess Plateau, changes in sediment provenance have been

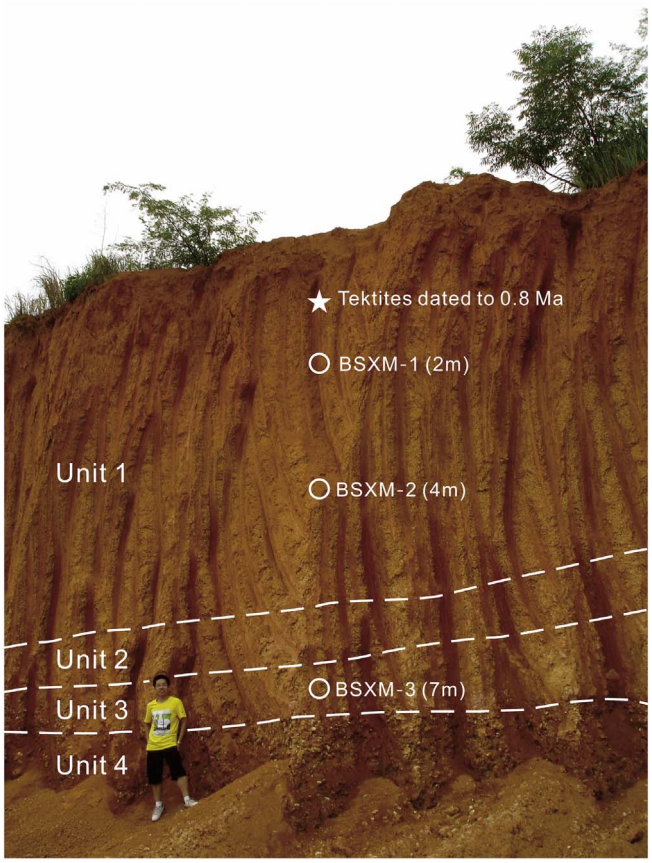

Fig. 2. Outcrop of the full Xiaomei red earth sequence, with locations of the sampling points and tektite $^{40}Ar/^{39}Ar$ age control point (Hou et al., 2000).

linked to glacial-interglacial climate variation (Xiao et al., 2012).

The Chinese Loess Plateau deposits have been investigated extensively with regard to their geographical setting, geochemical composition, provenance, and paleoclimatic significant (Gallet et al., 1996; Jahn et al., 2001; Ding et al., 2002; Jiang and Ding, 2010). These eolian sediments are sourced mainly in arid and semi-arid regions of central Asia and record alternations between cool/dry and warm/humid climate conditions corresponding closely to glacial and interglacial stages of the Pleistocene, respectively (Xiong et al., 2002). In subtropical southern China, geologically young (Pleistocene) red earth sediments are found widely in the areas of hills, river terraces, coalesced alluvial fans, and piedmont belts. Studies of the Pleistocene red earth sediments on the middle to lower reaches of the Yangtze River have confirmed that these deposits record paleoclimate patterns similar to those recorded in loess-paleosol sequences of the CLP in northern China (Hong et al., 2010). However, some studies have inferred an eolian origin for the upper part of the red earth sequence versus an alluvial origin for the middle and lower parts, reflecting secular changes in the sources and transport vectors of the red earth deposits, unlike for the CLP (Hu et al., 2003; Liu et al., 2014). For this reason, a better understanding of the provenance of the red earth sequence in southern China is essential for assessing its significance as a paleoclimatic record.

The geochemical composition and grain-size distribution pattern of red earth sediments in southern China have been employed for source identification in recent years. Because the red earth sediments show similarities in trace element composition (Ye et al., 2008; Qiao et al., 2011) and grain-size distributions (Xiong et al., 2002; Hu et al., 2005) to loess deposits of northern China, it has been inferred that they have a similar eolian origin. However, intensive chemical weathering under seasonally warm and humid conditions in southern China may have strongly modified the geochemical characteristics of the red earth deposits (Hong et al., 2013). Eolian transport distances may also have been much shorter for these deposits, as demonstrated for the Xiashu Loess in southern China (Zhang et al., 2005; Liu et al., 2014).

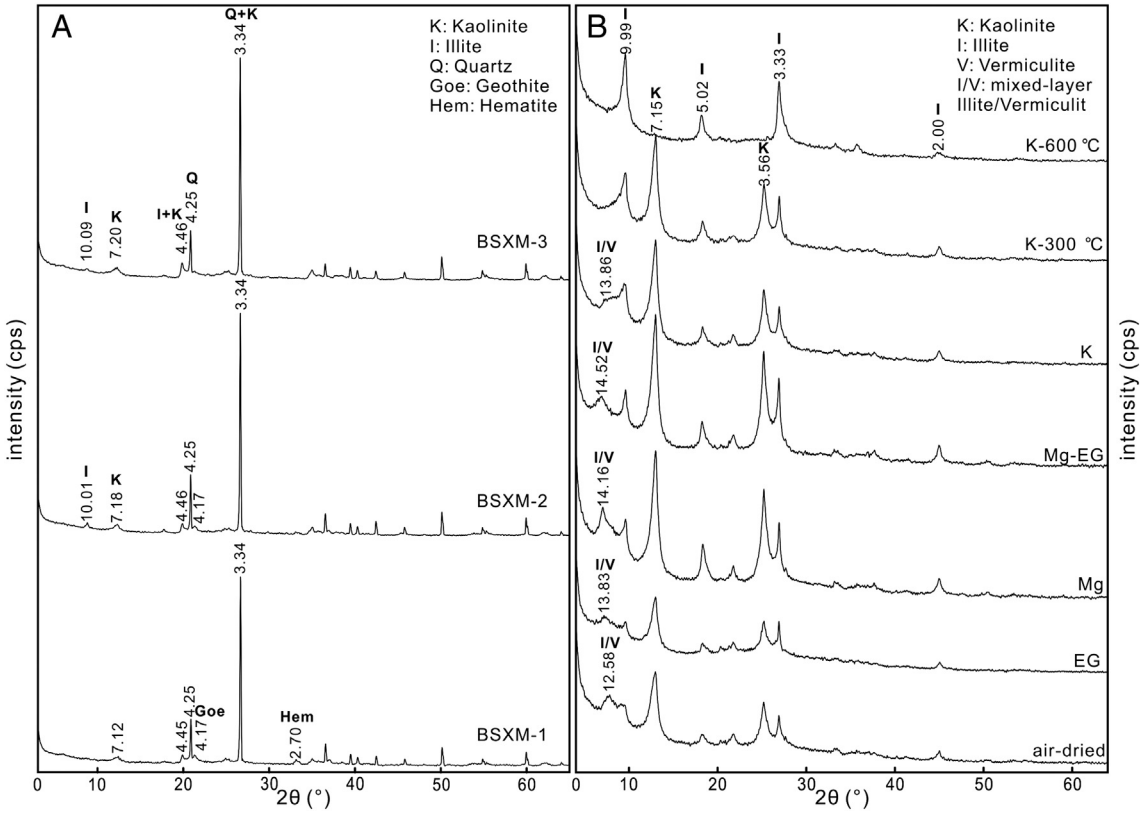

Fig. 3. XRD patterns of representative (A) bulk samples and (B) clay mineral separates for Sample BSXM-2.

Table 1
Whole-rock major element compositions of Xiaomei net-like red earth profile (wt%), Bose Basin.

Sample	SiO_2	TiO_2	Al_2O_3	Fe_2O_3	MnO	MgO	CaO	Na_2O	K_2O	P_2O_5	LOI
BSXM-1	58.31	1.17	15.94	14.29	0.03	0.32	0.03	0.17	1.07	0.24	8.75
BSXM-2	66.46	1.15	15.81	7.94	0.02	0.36	0.03	0.19	1.59	0.12	6.70
BSXM-3	73.50	1.40	13.43	4.77	0.03	0.34	0.05	0.17	1.29	0.07	5.38
Mean	66.09	1.24	15.06	9.00	0.03	0.34	0.04	0.18	1.32	0.14	6.94
UCC[a]	65.89	0.50	15.17	4.49	0.07	2.20	4.19	3.89	3.39	0.20	
PAAS[b]	62.80	1.00	18.90	6.50	0.11	2.20	1.30	1.20	3.70	0.16	
Loess[c]	62.89	0.58	12.59	4.81	0.09	3.84	10.91	1.67	2.32		
Paleosol[c]	67.28	0.66	13.54	5.50	0.09	2.50	5.81	1.79	2.49		

[a] Taylor and McLennan (1985).
[b] McLennan (1989).
[c] Ding et al. (2001).

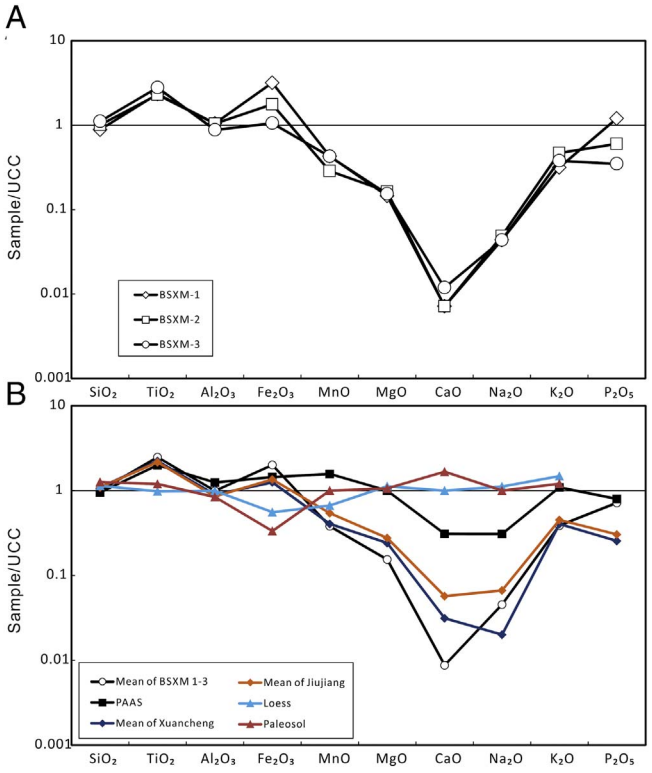

Fig. 4. UCC-normalized major-element distributions for (A) individual Xiaomei samples, and (B) average for all Xiaomei samples compared with upper continental crust (UCC) and post-Archean Australian shale (PAAS) from Taylor and McLennan (1985), CLP loess and paleosol from Ding et al. (2001), and Xuancheng and Jiujiang red earth sequences from Hong et al. (2013).

The abundance of detrital zircons and their resistance to chemical weathering make these grains useful for provenance studies (Belousova et al., 2002; Andersen, 2005). Analysis of single zircon crystals is considered a reliable method for determination of sediment provenance, especially for identification of large-scale source regions (Stevens et al., 2010; Újvári et al., 2012; Xie et al., 2012). In this study, the mineralogical and geochemical characteristics as well as the age distributions of detrital zircons of the red earth sediments at Xiaomei were investigated with the objective of constraining their provenance and formation processes.

2. Local geology and red earth sediments

The Bose Basin is a strike-slip extensional basin in Guangxi Zhuang Autonomous Region, southern China (Fig. 1) that formed during the Paleogene. The rapid uplift of the Tibetan Plateau in the mid-Pleistocene established the present geomorphic framework of southern China and also caused a widespread sedimentary hiatus to develop in the Guangxi area (Du and Xu, 2012). The sediments within the basin are mainly Permian to Triassic marine clastic and volcaniclastic strata and platform carbonates (Yang et al., 2012a), Paleogene clastic strata, and Quaternary alluvium and eluvium (Yuan et al., 2008). The climate was influenced by the East Asian summer monsoon (EASM), the East Asian winter monsoon (EAWM), and the Indian or South Asian monsoon (SAM). River terraces formed within the Bose Basin when the Youjiang River began to flow through it. Red earth sediments are present on all of the terraces throughout the study area. These paleosols formed in the subtropical monsoon system, being accretionary in nature and reflecting some degree of syndepositional pedogenesis under a warm, seasonally wet paleoclimatic conditions. They are distinctly different in terms of soil horizonation, color, and structure from the eolian deposits that accumulated concurrently on the CLP.

The section we studied is from the Xiaomei paleolithic site, located on the fourth terrace of the Youjiang River (Fig. 1A). According to $^{40}Ar/^{39}Ar$ dating of tektites, paleomagnetism, and fission track analyses, the fourth terrace is of late Early to early Middle Pleistocene age (~1.0–0.6 Ma) (Hou et al., 2000; Yuan et al., 2008; Wang and Bae, 2015). The Xiaomei section is ~8 m thick and can be divided into four lithological units that are distinguished by their color, vein characteristics, and inclusions (Fig. 2). The uppermost unit, Unit 1 (0–6.2 m), consists of brownish-red to brownish-yellow loam, with gray to white net-like veins distributed through the sediment matrix. The veins contain more Si and less Fe and Mn than the sediment matrix due to concentration of silica and removal of clay minerals through weathering. Tektites and paleolithic handaxes have been found at a level ~1 m below the present-day surface, which has been dated to ~0.8 Ma (Hou et al., 2000). Unit 2 (6.2–6.9 m) consists of brownish to yellow-brownish sandy loam containing white nodules. Unit 3 (6.9–7.4 m) consists of brownish-red silty loam with more extensively developed net-like veins relative to the overlying layer. The lowermost unit, Unit 4 (7.4–8 m), consists of brownish-red to brownish-yellow silty loam with white clay nodules and large numbers of sub-rounded and rounded pebbles of locally sourced material. Samples were collected at depths of 2, 4, and 7 m within the section for geochemical and provenance analysis of the Xiaomei red earth sediments.

3. Methods

3.1. Clay mineralogy analysis

The bulk samples were dried at 40 °C overnight, and then ground to finer than 0.74 μm using an agate mortar. XRD analysis was performed on a Panalytical diffractometer at the Key Laboratory of Geological Processes and Mineral Resources (GPMR) of China University of

Geosciences (CUG), Wuhan, over the range of 3° to 65° 2θ with a scan rate of 4° 2θ min^{-1} and a step size of 0.02° 2θ. The clay mineral fraction was concentrated by the sedimentation method, and clay minerals were identified based on their characteristic diffraction peaks (Hong et al., 2010).

3.2. Major, trace, and rare earth element analyses

Loss-on-ignition (LOI) was measured prior to generating fused glass pellets. Major element analysis was performed on an XRF-1800 SHIMADZU sequential X-ray fluorescence (XRF) spectrometer with a rhodium tube and a 2.5 kW generator at the Key Laboratory of Biogeology and Environmental Geology (BGEG) of CUG. The detection limit was ~0.01 wt% with a measurement error of < 1%. A second aliquot of each sample was placed in a Teflon container and dissolved in a mixture of hydrofluoric acid and nitric acid in preparation for trace and rare earth element measurements. Analyses were performed on an Agilent 7500a ICP-MS instrument at the GPMR of CUG following the analytical procedures of Liu et al. (2008a). The analytical precision was < 4% for REEs and Y, and 5–10% for other trace elements.

3.3. Sr and Nd isotope analyses

Two resin columns (AG50w × 8 and Dowe × 50w × 8) were used to separate Rb, Sr, and trace elements after dissolution in hydrochloric acid. Sm and Nd were separated by an ion exchange column following the procedure of Jahn and Condie (1995). Isotope measurements were conducted on a Triton Ti thermal ionization mass spectrometer (TIMS) at GPMR of CUG. Isotope ratios of $^{87}Sr/^{86}Sr$ and $^{143}Nd/^{144}Nd$ were standardized respectively based on $^{86}Sr/^{88}Sr = 0.1194$ and $^{146}Nd/^{144}Nd = 0.7219$. The standards NBS987 and La Jolla Nd_2O_3 were repeatedly measured during the test period to calibrate the instrument. Average values of the isotope ratios of $^{87}Sr/^{86}Sr$ and $^{143}Nd/^{144}Nd$ were 0.71026 ± 5 (2σ) and 0.511845 ± 10 (2σ).

3.4. Detrital zircon U-Pb isotopic analyses

Zircon grains (> 1000 per sample) were picked from the non-magnetic heavy mineral assemblage of samples after magnetic and heavy-liquid separation. Grains from each sample were arranged in rows, embedded in epoxy resin, and polished to two-thirds of their original diameter for dating analysis. Cathodoluminescent, transmitted-light, and reflected-light images of each zircon grain were taken to ensure that the laser spots for dating were located in the magmatic portion of the crystal and contained no inclusions or fissures. Detrital zircon U-Pb dating was conducted using a laser ablation system and an inductively coupled plasma source mass spectrometer (LA-ICP-MS, Agilent 7500a) at GPMR of CUG. Repeated measurements of the external zircon standards GEMOC GJ-1 (608.5 ± 15 Ma) (Jackson et al., 2004) and 91,500 (1062 ± 4 Ma) (Wiedenbeck et al., 1995) were used for calibration and calculation of depth-dependent elemental fractionations between Pb, Th, and U. The trace element compositions of zircon crystals were calibrated against multiple reference materials combined with the Si in NIST 610 glass as an internal standard (Liu et al., 2010). Pb was corrected using the method proposed by Andersen (2002). The detailed analytical procedures including off-line calculations, time-drift corrections, U-Pb dating, and quantitative calibration of trace elements were performed by the ICPMS DataCal program (Liu et al., 2008b, 2010). Zircon U-Pb age concordia diagrams and probability density plots were generated using Isoplot/Ex version 3.41 (Ludwig, 2006).

To approach the true probability density distribution of detrital zircon dates in each sample, 100 points with a laser spot diameter of 32 μm were analyzed to guarantee statistical significance (Andersen, 2005). The $^{206}Pb/^{238}U$ method was used to calculate crystals ages < 1000 Ma, and the $^{207}Pb/^{206}Pb$ method for crystal ages > 1000 Ma.

Table 2
Whole-rock trace element compositions of Xiaomei net-like red earth profile (ppm), Bose Basin.

Sample	Rb	Ba	Th	U	Nb	Ta	La	Ce	Pb	Pr	Sr	Nd	Zr	Hf	Sm	Eu	Gd	Tb	Dy	Y	Ho	Er	Tm	Yb	Lu
BSMX-1	72.8	172.7	17.0	4.4	18.1	1.3	33.5	61.1	27.9	6.8	42.8	24.0	263.0	6.8	4.0	0.7	3.4	0.6	4.0	26.0	0.9	2.6	0.4	2.7	0.4
BSMX-2	89.6	231.8	14.4	3.6	17.6	1.2	34.3	66.3	20.4	7.5	47.1	27.8	308.1	7.9	5.2	1.0	4.2	0.7	4.5	27.3	0.9	2.7	0.4	2.9	0.4
BSMX-3	76.5	196.5	11.0	2.6	10.0	0.5	26.4	55.6	14.8	6.1	34.8	22.4	262.4	6.8	4.1	0.8	3.6	0.6	3.8	23.5	0.8	2.4	0.4	2.4	0.3
Mean	79.6	200.3	14.2	3.5	15.2	1.0	31.4	61.0	21.0	6.8	41.6	24.7	277.8	7.2	4.4	0.8	3.7	0.6	4.1	25.6	0.9	2.6	0.4	2.6	0.4
UCC[a]	112	550	10.7	2.8	12	1	30	64	17	7.1	350	26	190	5.8	4.5	0.88	3.8	0.64	3.5	22	0.8	2.3	0.33	2.2	0.32
PAAS[b]	160	650	14.6	3.1	19		38.2	79.6	20	8.83	200	33.9	210	210	5.55	1.08	4.66	0.774	4.68	27	0.991	2.85	0.405	2.82	0.433
Loess[c]	125	578	13.9	2.97	16.3	1.25	33.4	66.8	35.7	7.38	113	28	151	4.69	5.27	1.02	4.37	0.75	4.42	22.6	0.89	2.52	0.39	2.51	0.38
Paleosol[c]	137.00	543.00	14.00	2.92	16.60	1.29	34.50	67.60	32.00	7.64	104	28.9	152.00	4.55	5.44	1.05	4.51	0.75	4.32	23.10	0.87	2.51	0.39	2.48	0.37

[a] Taylor and McLennan (1985).
[b] McLennan (1989).
[c] Hao et al. (2010).

Table 3
Whole-rock rare element compositions of Xiaomei net-like red earth profile (ppm), Bose Basin.

Sample	La	Ce	Pr	Nd	Sm	Eu	Gd	Tb	Dy	Ho	Er	Tm	Yb	Lu
BSMX-1	33.5	61.1	6.8	24.0	4.0	0.7	3.4	0.6	4.0	0.9	2.6	0.4	2.7	0.4
BSMX-2	34.3	66.3	7.5	27.8	5.2	1.0	4.2	0.7	4.5	0.9	2.7	0.4	2.9	0.4
BSMX-3	26.4	55.6	6.1	22.4	4.1	0.8	3.6	0.6	3.8	0.8	2.4	0.4	2.4	0.3
Mean	31.4	61.0	6.8	24.7	4.4	0.8	3.7	0.6	4.1	0.9	2.6	0.4	2.6	0.4
UCC[a]	30	64	7.1	26	4.5	0.88	3.8	0.64	3.5	0.8	2.3	0.33	2.2	0.32
PAAS[b]	38.2	79.6	8.83	33.9	5.55	1.08	4.66	0.774	4.68	0.991	2.85	0.405	2.82	0.433
Loess[c]	33.4	66.8	7.38	28	5.27	1.02	4.37	0.75	4.42	0.89	2.52	0.39	2.51	0.38
Paleosol[c]	34.50	67.60	7.64	28.9	5.44	1.05	4.51	0.75	4.32	0.87	2.51	0.39	2.48	0.37

[a] Taylor and McLennan (1985).
[b] McLennan (1989).
[c] Hao et al. (2010).

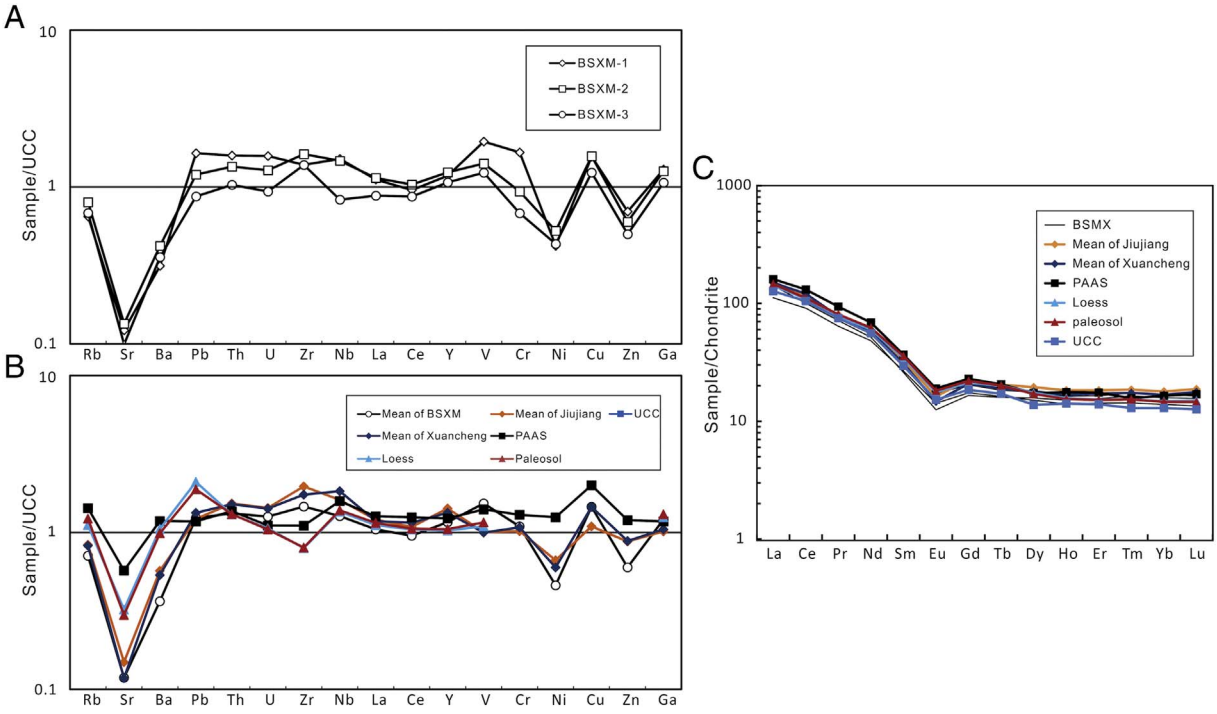

Fig. 5. (A–B) UCC-normalized trace-element and (C) chondrite-normalized rare earth element distributions for individual Xiaomei samples, and average for all Xiaomei samples compared with upper continental crust (UCC) and post-Archean Australian shale (PAAS) from Taylor and McLennan (1985), CLP (Xifeng) loess and paleosol from Hao et al. (2010) and Ding et al. (2001), and Xuancheng and Jiujiang red earth sequences from Hong et al. (2013). Normalizations based on chondritic composition of Taylor and McLennan (1985) and primitive mantle composition of Sun and McDonough (1989).

Results with an age consonance lower than 90% were discarded owing to their unreliability.

4. Results

4.1. Mineralogic composition of red earth sediments

The XRD patterns of the bulk samples show that the red earth sediments contain similar mineral components in all units of the Xiaomei profile. Quartz and clay minerals are ubiquitous, and hematite and goethite are present in minor amounts in BSXM-1 but were not observed in BSXM-3 (Fig. 3A).

The 10–14 Å peaks in the air-dried clay slides shifted to slightly lower angles after ethylene glycol (EG) saturation, indicating the presence of expandable components in the mixed-layer clay minerals. These peaks expanded to ~14 Å after magnesium (Mg) and magnesium-ethylene glycol treatment (Mg-EG), and collapsed to 10 Å after potassium saturation (K) and heating (to 600 °C), when the intensity of the ~10 Å and ~5 Å peaks measurably increased, suggesting the presence of mixed-layer illite/vermiculite (I/V) (Fig. 3B). The intensities of peaks at ~10 Å, ~5 Å and ~3.3 Å showed no change among the air-dried, saturated and heat-treated samples, whereas the ~7.2 Å peak disappeared, suggesting the presence of illite and kaolinite in the samples.

4.2. Major element composition

Table 1 gives average concentrations for major elements in the Xiaomei red earth sequence, along with comparative data for the red earth sequences at Xuancheng and Jiujiang, loess-paleosols from the CLP, and PAAS. All data are normalized to UCC (Taylor and McLennan, 1985). All samples from Xiaomei yield similar major element distributions with only minor differences (Fig. 4A). The relatively high LOI values reflect high concentrations of clay minerals, iron hydroxides,

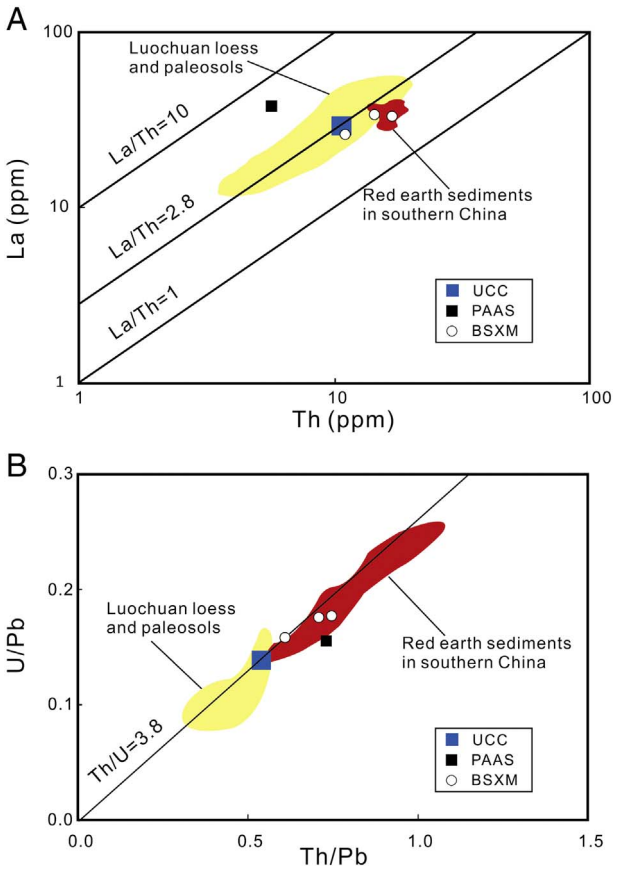

Fig. 6. (A) La vs. Th, and (B) Th/U vs. U/Pb. Uniform La/Th and Th/U ratios are consistent with continental provenance of Xiaomei red earth. Red earth data from Hong et al. (2013), Luochuan loess and paleosol data from Gallet et al. (1996), and UCC data Taylor and McLennan (1985).

Table 4
Isotopic ratios of Sr and Nd of Xiaomei net-like red earth profile, Bose Basin.

Sample	$^{87}Sr/^{86}Sr$	$^{143}Nd/^{144}Nd$	$^{147}Sm/^{144}Nd$	$\varepsilon_{Nd}(0)$
BSXM-1	0.721246	0.512143	0.099951226	− 9.646081676
BSXM-2	0.725232	0.512151	0.112245842	− 9.49128062
BSXM-3	0.725483	0.512169	0.110320738	− 9.139958473

$\varepsilon_{Nd}(0) = ((^{143}Nd/^{144}Nd)s / (^{143}Nd/^{144}Nd)_{CHUR} - 1) * 10^4$, where$(^{143}Nd/^{144}Nd)_{CHUR} = 0.512638$.

and soil organic matter. The SiO_2 content shows notable variation (from 58.3 to 73.5 wt%) and is negatively correlated with Al_2O_3 content (from 13.4 to 15.9 wt%). The TiO_2 content (1.17–1.40 wt%) is high owing to intense chemical weathering. The Fe_2O_3(t) content (4.8–14.3 wt%) varies strongly among different horizons in the Xiaomei section but exhibits an overall decreasing trend from top to bottom of the section. The CaO content is generally low, but eluviation has resulted in downward increases within the section. The Na_2O (0.17–0.19 wt%) and K_2O contents (1.07–1.59 wt%) show similar trends, decreasing from top to bottom. Alkali metals commonly show strong mobility during weathering, but despite the warm and humid climate conditions of the Bose Basin, Na_2O and K_2O contents at Xiaomei remain high. The MgO content of the samples is relatively invariant (0.30–0.34 wt%). These geochemical results are consistent with a clay mineral assemblage consisting mainly of illite, vermiculite, and kaolinite.

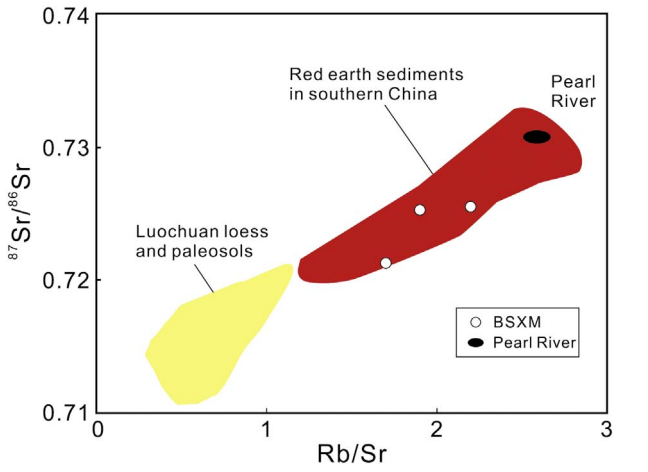

Fig. 7. $^{87}Sr/^{86}Sr$ vs. Rb/Sr. Linear array of Xiaomei samples indicates compatibility with Pearl River sediments. CLP loess and Pearl River sediment data from Boulay et al. (2005) and red earth data from Hong et al. (2013).

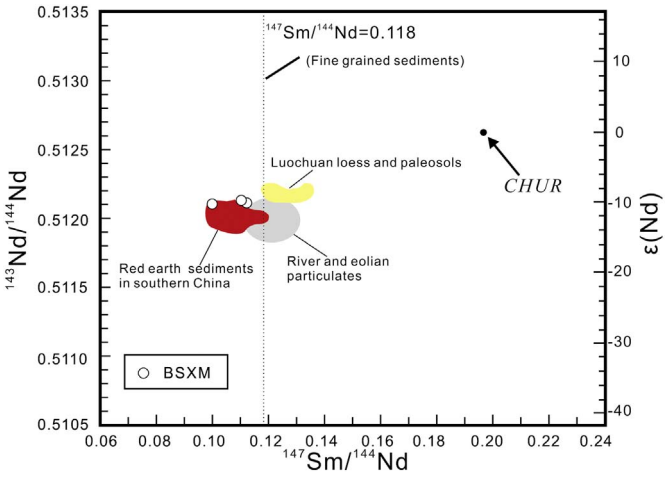

Fig. 8. $^{143}Nd/^{144}Nd$ vs. $^{147}Sm/^{144}Nd$. Xiaomei samples plot close to other red earth sequences in southern China (from Hong et al., 2013) and fine-grained sediments (from Jahn and Condie, 1995) but far from CLP (Luochuan) loess-paleosols (after Gallet et al., 1998). CHUR = chondritic uniform reservoir.

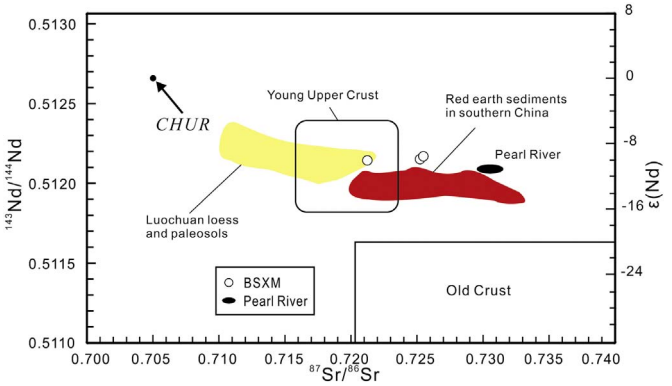

Fig. 9. $^{143}Nd/^{144}Nd$ vs. $^{87}Sr/^{86}Sr$. Xiaomei samples plot close to other red earth sediments in southern China. Red earth data from Hong et al. (2013), CLP loess data from Boulay et al. (2005), and young upper crust data from Gallet et al. (1998). CHUR = chondritic uniform reservoir.

Fig. 10. Representative cathodoluminescent (CL) images of Xiaomei detrital zircons with laser spots (red circles) and corresponding ages. (For interpretation of the references to color in this figure legend, the reader is referred to the web version of this article.)

4.3. Trace and rare earth element composition

Tables 2 and 3 give the trace element and rare earth element concentrations of the Xiaomei samples, the red earth sequences at Xuancheng and Jiujiang, the loess-paleosols of the CLP, PAAS, and UCC. All data were normalized to primitive mantle and chondrites (Fig. 5). The relationship of La-Th and Th-U/Pb is presented in Fig. 6. All Xiaomei samples exhibit similar trace element patterns, with only a slight depletion of Ta at the base of the section relative to overlying samples. All of the Xiaomei samples have notable depletions of Ba and Sr, which are similar to the Xuancheng and Jiujiang red earth sediments. In general, the rare earth element distribution pattern of the Xiaomei samples is characterized by relative enrichment of light rare earth elements (LREEs), depletion of heavy rare earth elements (HREEs), and a negative Eu anomaly.

4.4. Sr-Nd isotopic compositions

The Xiaomei samples yield Sr and Nd concentrations of 34–47 ppm and 22–27 ppm, respectively, and $^{87}Sr/^{86}Sr$ values of 0.7212–0.7254 (Table 4). Sr and Nd are relatively abundant in Sample BSXM-2 compared to Samples BSXM-1 and -3, and the $^{87}Sr/^{86}Sr$ ratio gradually decreases from the top to the bottom of the section. In a $^{87}Sr/^{86}Sr$ vs. Rb/Sr crossplot, the Xiaomei samples fall close to those of red earth sediments in southern China but far from the CLP samples (Fig. 7). The $^{143}Nd/^{144}Nd$ vs. $^{147}Sm/^{144}Nd$ and $^{143}Nd/^{144}Nd$ vs. $^{87}Sr/^{86}Sr$ crossplots show a similar pattern of results (Figs. 8–9).

4.5. Detrital zircon U-Pb ages

Detrital zircon LA-ICP-MS data are given in Supplementary Table 5,

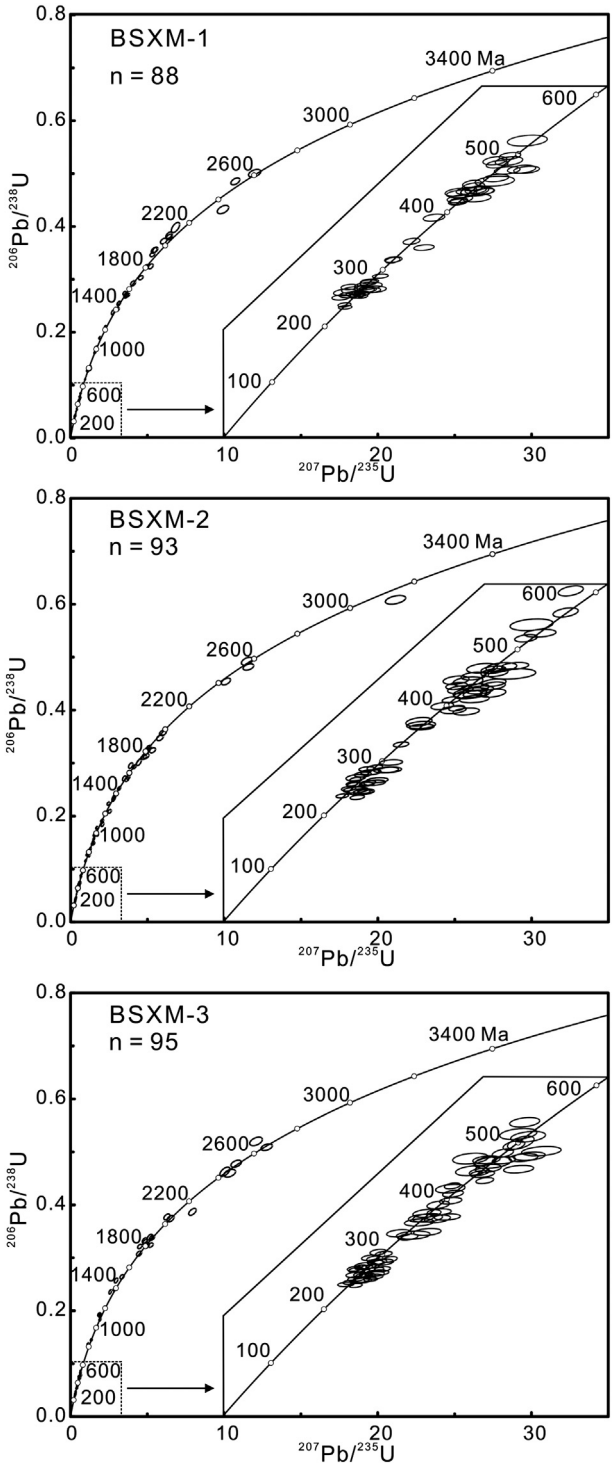

Fig. 11. U-Pb isochrons of showing results for concordant detrital zircons in the three Xiaomei samples; the inset in each panel show details of the 0–600 Ma portion of the isochron.

and images of representative zircon grains are shown in Fig. 10. Zircon grains exhibited similar size ranges (~50 to 100 μm) but different crystal forms in the three samples. Sample BSXM-1 and -2 contains mainly euhedral crystals, whereas Sample BSXM-3 contains primarily round and anhedral crystals. Most of the analyzed crystals plot on or adjacent to the isochron, and only a few crystals show evidence of Pb loss (Fig. 11). The U-Pb ages range from the Archean (3191 Ma) to the Early Triassic (234 Ma). Of the 300 ages generated for Xiaomei zircons, 276 met the criterion of 90% consonance and were incorporated in the age probability density distribution (Fig. 12), together with zircon age data from earlier studies (Wang et al., 2007a, 2007b, 2011; Stevens et al., 2010; Xu et al., 2011; Pullen et al., 2011; Li et al., 2011; Yang et al., 2012a, 2012b, 2014).

The Xiaomei samples yielded age probability density distributions that are similar to those of the comparative samples from earlier studies. All show a multi-peak distribution with zircon ages concentrated in three intervals: 240–280 Ma, 420–480 Ma, and 900–1000 Ma, with the first two intervals (centered at ~260 and ~440 Ma) yielding the larger peaks at Xiaomei. Smaller and/or broader peaks are present at ~360 Ma, 1320–1640 Ma, 1700–2000 Ma, and ~2500 Ma (Fig. 12), indicating that the Xiaomei red earth has a multi-source parent material. Subtle differences exist in the relative intensity of these age peaks between the deposits: the relative height of the ~260-Ma peak in Sample BSXM-3 is larger than in Samples BSXM-1 and -2; the ~360-Ma peak appears clearly in Sample BSXM-3 but is not apparent in Samples BSXM-1 and -2; and the intensity of the ~440-Ma peak is higher in Samples BSXM-1 and -2 than in Sample BSXM-3.

The age distribution pattern indicates that crystals from the Late Ordovician to Middle Triassic periods are mostly euhedral, particularly those dated to ~260 Ma. These detrital zircon crystals have characteristics of magmatic origin according to their Th/U ratios and cathodoluminescence (CL) images (Corfu et al., 2003; Hoskin and Schaltegger, 2003).

Compared with younger zircon crystals, those of early Furongian-late Mesoproterozoic (485–1600 Ma) age exhibit varied morphological features. These crystals may have experienced intense weathering and multiple stages of recycling. Most of these crystals exhibit subhedral to euhedral form, with oscillatory zones of uneven thickness and local overgrowths (Fig. 10). The Th/U ratios of these crystals vary over a wide range (0.08–3.19), indicating that they might be of both magmatic and metamorphic origin.

The zircon crystals from the Paleoproterozoic-Archaean (1600–3500 Ma) are much less numerous than younger zircons, and thus no age peaks can be discerned. These crystals are mostly round or broken in shape, and they are found scattered in layers throughout the soil profile. Cathodoluminescence images indicate that these crystals have complicated internal zonation, a xenolith core, and local overgrowths (Belousova et al., 1998; Rubatto and Gebauer, 2000). Their wide range of Th/U ratios (0.10–1.47) indicates that they may have both magmatic and metamorphic origins.

4.6. REE distribution patterns of detrital zircons

The concentrations of trace elements in the Xiaomei zircons are given in Supplementary Table 6, and their chondrite-normalized values are shown in Fig. 13. Zircon crystals can be divided into three types according to their rare earth element (REE) distribution patterns: (1) normal magmatic distribution (n = 249), (2) flat HREE distribution (n = 9), and (3) flat LREE distribution (n = 18). The normal magmatic group tends to show pronounced Ce enrichment and Eu depletion, which is consistent with an anorthositic parent rock without the presence of garnet, i.e., typical of material derived from the lower continental crust (Belousova et al., 2002; Hoskin and Schaltegger, 2003; Hanchar and Van, 2007). The flat HREE group exhibits variable degrees of MREE enrichment and/or HREE depletion, and most samples show a limited negative Eu anomaly. The flat LREE group exhibits pronounced LREE-enrichment and a weaker positive Ce anomaly than the normal magmatic group [$(Sm/La)_N < 2.1$, $(Ce/Ce^*)_N < 2.1$]. Based on Th/U ratios, REE patterns, and CL images, we infer that nearly all zircons show characteristics of magmatic origin (the exceptions being three crystals with homogenized metamorphic zones). These groups show distinct age differences: the flat LREE group mainly yields ages of 240–280 Ma and 420–480 Ma, and the flat HREE group ages of 890–1200 Ma. The differences in REE characteristics of zircon crystals

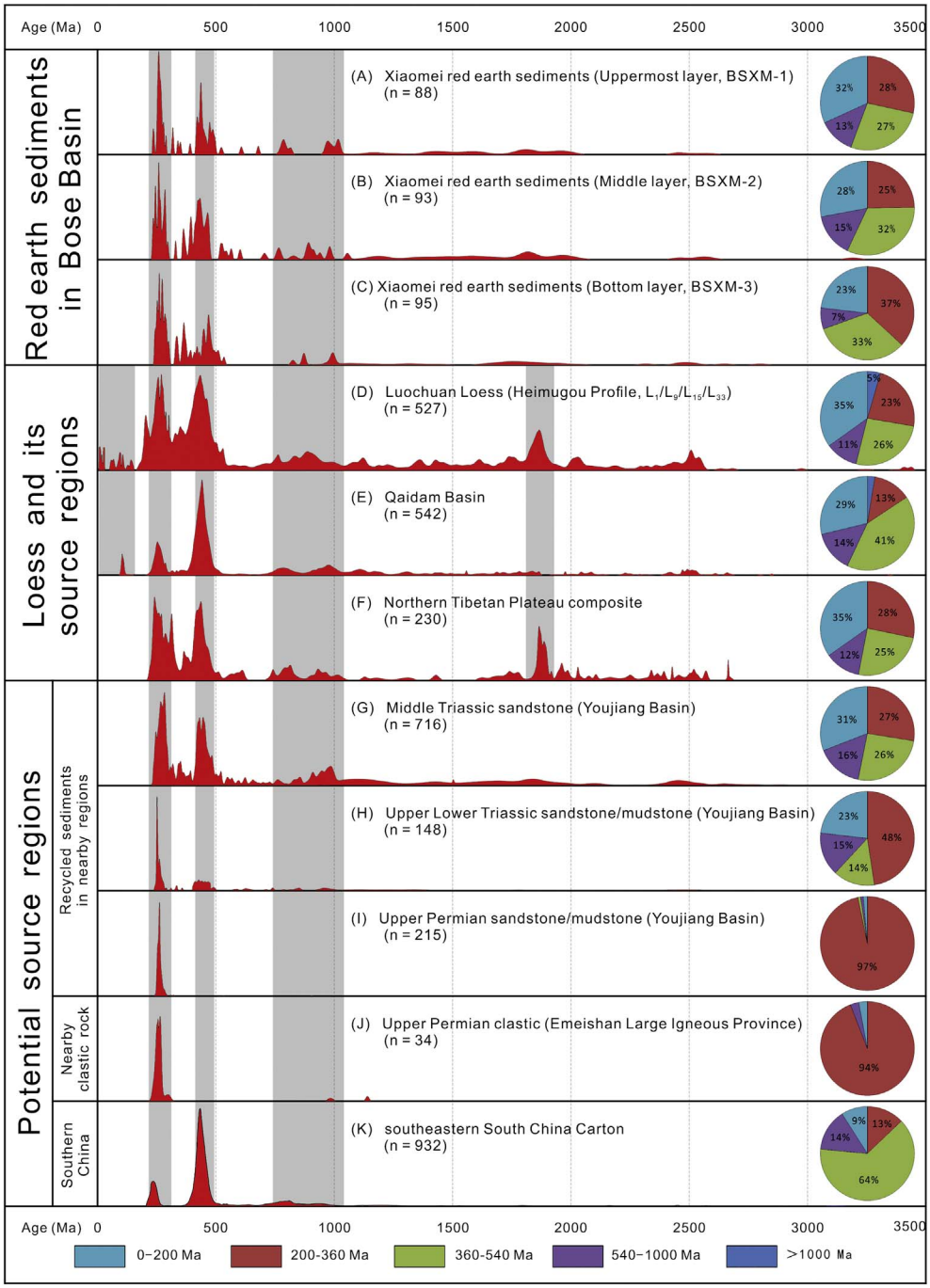
Age (Ma) 0 500 1000 1500 2000 2500 3000 3500
Red earth sediments in Bose Basin
(A) Xiaomei red earth sediments (Uppermost layer, BSXM-1) (n = 88)
(B) Xiaomei red earth sediments (Middle layer, BSXM-2) (n = 93)
(C) Xiaomei red earth sediments (Bottom layer, BSXM-3) (n = 95)
Loess and its source regions
(D) Luochuan Loess (Heimugou Profile, L1/L9/L15/L33) (n = 527)
(E) Qaidam Basin (n = 542)
(F) Northern Tibetan Plateau composite (n = 230)
Potential source regions
Recycled sediments in nearby regions
(G) Middle Triassic sandstone (Youjiang Basin) (n = 716)
(H) Upper Lower Triassic sandstone/mudstone (Youjiang Basin) (n = 148)
(I) Upper Permian sandstone/mudstone (Youjiang Basin) (n = 215)
Nearby clastic rock
(J) Upper Permian clastic (Emeishan Large Igneous Province) (n = 34)
Southern China
(K) southeastern South China Carton (n = 932)
0–200 Ma
200-360 Ma
360-540 Ma
540–1000 Ma
>1000 Ma

Fig. 12. Probability-density distributions and pie-charts of U-Pb ages of detrital zircons from the Xiaomei samples (A, B, C), Luochuan loess (D), Quaternary alluvium and wind-eroded Pliocene–Pleistocene lacustrine strata of Qaidam Basin (E), and Triassic sandstones of northern Tibetan Plateau (F) from Pullen et al. (2011); Middle Triassic sandstone of Youjiang Basin (G) from Yang et al. (2012a); upper Lower Triassic siltstone and mudstone (H) and Upper Permian sandstone and mudstone of Youjiang Basin (I) from Yang et al. (2012b, 2014); Upper Permian clastic samples of eastern Emeishan large igneous province (J) from He et al. (2007); and detrital grains of southeastern South China Craton (K) from Li et al. (2011), Wang et al. (2007a, 2007b, 2011), and Xu et al. (2011).

at Xiaomei are thus probably derived from their parent materials.

Most zircons have low Nb/Hf and Th/U ratios and high Th/Nb and Hf/Th ratios, placing them in the field of arc-related or orogenic origin (Fig. 14). Only a few crystals of Precambrian age fall in the region of intraplate or anorogenic origin (Fig. 14), suggesting that zircons in the Xiaomei red earth sediments are primarily of volcanic origin (Hoskin and Ireland, 2000).

5. Discussion

5.1. Geochemical characteristics of Xiaomei red earth sediments

The Xiaomei samples all show similar major element distribution patterns on a UCC-normalized plot (Fig. 4), consistent with other red earth sediments in southern China. The concentrations of SiO_2, Al_2O_3, and Fe_2O_3 (t) in these samples are similar to or slightly higher than those for UCC, whereas TiO_2 is notably enriched, especially for Sample BSXM-3. The chemical index of alteration (CIA), which is a useful proxy for the degree of chemical weathering of sediments and soils (Nesbitt and Young, 1982), is defined as the molar ratio of $Al_2O_3/(Al_2O_3 + CaO^* + Na_2O + K_2O) \times 100$, where CaO* is the amount of CaO in silicates. The unusually high SiO_2 and Al_2O_3 contents and CIA values (88–91) of the Xiaomei samples reflect intense chemical weathering. The geochemistry of the samples is clearly related to their mineral composition, which is dominated by the clay minerals kaolinite, illite, and mixed-layer illite/vermiculite (I/V) (Fig. 3). Samples from the upper part of the profile have relatively higher Fe_2O_3 (t) contents, consistent with the presence of hematite and goethite. Compared to PAAS and loess-paleosols of northern China (Ding et al., 2001; Hao et al., 2010), the Xiaomei red earth is characterized by lower MnO_2, CaO, K_2O, and Na_2O contents, reflecting intense leaching of alkali cations through weathering under warm and humid climate

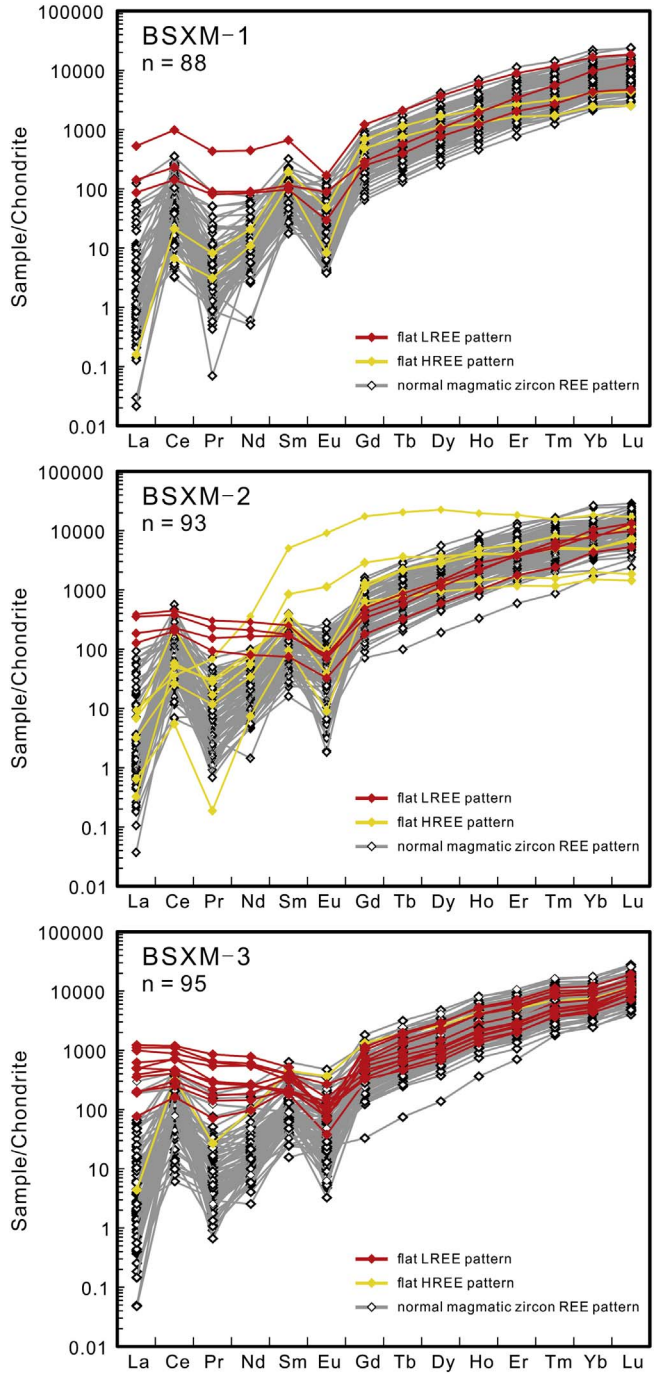

Fig. 13. Chondrite-normalized REE distributions of zircons in the three Xiaomei red earth samples.

conditions in southern China during the Pleistocene.

Ba and Sr tend to be mobilized under conditions of intense chemical weathering (Jahn et al., 2001). Relative to primitive mantle, all of the red earth sediment sections of southern China (i.e., Xiaomei as well as Xuancheng and Jiujiang) exhibit depletion of Rb, Ce, Ba and Sr and enrichment of Th, U, Pb, Nd, Zr, and Hf. Depletion of Ba and Sr and enrichment of resistate elements such as Zr indicate that the red earth sediments in southern China have experienced more intense chemical weathering than the loess-paleosol sections of the CLP in northern China (Hong et al., 2013).

The trace elements La and Th are relatively immobile during weathering and transport (Holland, 1978). The Xiaomei samples yield La/Th ratios of about 2.8 (Fig. 6A), close to those of other red earth sediments from southern China and also within the range of samples from the CLP and UCC.

The Th/U ratios of Xiaomei samples are close to 4.0, similar to other red earth sediments in southern China but slightly higher than the 3.8 of UCC (Fig. 6B). Whereas Th is relatively insoluble and has a low concentration (0.1–0.2 ppb) in river water, U is similar to the alkali cations in being mobile during intense chemical weathering. The U/Pb vs. Th/Pb crossplot confirms that the parent materials of the Xiaomei sediments experienced mixing in transport (Fig. 6B). The Xiaomei samples also have a consistent chondrite-normalized REE distribution pattern that is similar to those of the CLP, UCC, and PAAS (Fig. 5C), consistent with mixing prior to deposition. Eu is relatively immobile during weathering and transport relative to other trace elements (McLennan, 1989). The Eu/Eu* ratios of the Xiaomei samples are 0.86–0.94, with a mean value of 0.92, similar to those of the CLP, UCC, PAAS, and other red earth sediments in southern China (e.g., 0.85 for Jiujiang and 0.83 for Xuancheng). These similarities suggest that the Xiaomei red earth sediments represent well-mixed, multi-cyclic deposits derived from upper crustal materials.

The Sr isotopic composition of sediments is related to parent materials, particle size, and chemical weathering intensity (Goldstein and Jacobsen, 1987; Blum et al., 1993). The relatively high $^{87}Sr/^{86}Sr$ ratios of the Xiaomei samples fall within the field of red earth sediments in southern China, particularly those of Pearl River sediments, but display differences from those of the CLP loess in northern China (Fig. 7). The $^{87}Sr/^{86}Sr$ ratio increases as the degree of chemical weathering increases, due to preferential release of radiogenic Sr from silicate minerals (Hong et al., 2013). The relatively high CIA (88–91) and $^{87}Sr/^{86}Sr$ (0.7212–0.7254) of the Xiaomei samples are similar to those of red earth deposits from the middle to lower reaches of the Yangtze River, and their relatively high Rb/Sr ratio is also typical of intensely weathered fluvial sediments (Yang et al., 2004).

The Sm-Nd isotopic composition of sediments is inherited from that of the parent rock and, thus, can serve as a fingerprint for a particular sediment source area (Goldstein et al., 1984; Bronger and Heinkele, 1990; Gallet et al., 1998; Weldeab et al., 2002). A crossplot of $^{143}Nd/^{144}Nd$ vs. $^{87}Sr/^{86}Sr$ shows that the Xiaomei samples fall close to the Xuancheng and Jiujiang red earth deposits of the lower Yangtze River but far from the eolian deposits of the CLP (Fig. 9). Compared to fluvial sediments of small rivers, those of large rivers normally exhibit a narrower $\varepsilon_{Nd}(0)$ range, suggesting the effects of greater mixing of material derived from multiple sources (Goldstein et al., 1984; Goldstein and Jacobsen, 1987). The Xiaomei samples exhibit a comparatively narrow $\varepsilon_{Nd}(0)$ range (-9.14 to -9.65), consistent with a mainly well-mixed fluvial source with only limited inputs of eolian material.

5.2. Provenance of Xiaomei red earth sediments

The similarity of age patterns for all Xiaomei samples suggests that the provenance of detrital materials to the study site on the fourth terrace of the Youjiang River was stable throughout the interval of red earth formation. The zircon age distribution patterns are effectively identical in all samples, with peaks at ~260 and ~440 Ma and scattered Neoproterozoic ages (Fig. 12). Zircons of middle Indosinian age (~240–280 Ma) are more abundant than those of Caledonian age (~420–480 Ma), especially for Sample BSXM-3 (Fig. 12C). Similar age peaks for the CLP loess in northern China were used to infer sediment provenance: a ~440 Ma peak is thought to reflect derivation of materials from the Qaidam Basin in Qinghai Province (northwestern China), possibly from the Qilian Mountains (Pullen et al., 2011), and transportation via the Asian winter monsoon to inland China. The CLP loess also exhibits peaks at ~870, ~1860, and ~2500 Ma that are characteristic of eolian deposits originating from the northern Tibetan Plateau, but these peaks do not appear in the Xiaomei samples (Fig. 12D, F). Another potential source region of eolian sediments in northwestern China is the central Asian orogenic belt, which is known

to yield a dominant zircon age peak at ~400–200 Ma with smaller peaks at ~200–100 Ma and ~600–400 Ma (Che and Li, 2013). However, crystals younger than 200 Ma were not observed in the Xiaomei samples (Fig. 12A–C), which is inconsistent with material of central Asian origin.

Magmatic and metamorphic rocks with ages of 1000–2500 Ma are rare on the South China Craton (Fig. 12K). Zircons of these ages are found mainly in the Statherian-Orosirian igneous rocks of the Qinling-Dabie tectonic province, the Cathaysia Block, and lower Paleozoic clastic rocks of the southeastern Yangtze Block (Yao et al., 2011). These igneous rocks, together with clastic formations in the eastern Youjiang Basin, were probably the main parent materials of the red earth sediments found throughout the Bose region, as also suggested by paleocurrent evidence showing west-northwestward transport of fluvial sediments in Middle Triassic formations of the Youjiang Basin (Yang et al., 2012a). Proterozoic metamorphic rocks with ages of 1100–1300 Ma and 1700–1900 Ma around Kunming, Yunnan Province, in the northwestern part of the Bose Basin, might also be sources of the red earth sediment at Xiaomei (Wang et al., 2012).

The Beiliu-Chongzuo-Guangxi orogeny during the late Ordovician to late Silurian in Guangxi Zhuang Autonomous Region caused large-scale denudation of Ordovician and Silurian formations in the Youjiang area (Du and Xu, 2012). However, the Qingfang Belt of southern Guangxi Province was not influenced by Caledonian-age tectonism, and Silurian to early Devonian strata were continuously deposited there. Granites with an age of ~440 Ma in southeastern Yunnan Province (e.g., the Laojunshan-Song Chay Dome) could also be a potential source, taking into account evidence for west-northwestward paleocurrents in Middle Triassic strata of the Youjiang Basin (Yang et al., 2012a) (Fig. 1C).

A thick succession of Upper Permian-Middle Triassic clastic strata is found widely across the Bose region (Fig. 1B). Within this succession, turbidites yield a consistent zircon U-Pb age distribution (Yang et al., 2012a), with dominant age peaks at 240–300 Ma, 420–480 Ma, and 900–1200 Ma, and minor peaks at 300–410 Ma and 550–90 Ma (Fig. 12G), similar to the age distribution of Xiaomei zircons. Moreover, the chondrite-normalized REE distributions of Xiaomei zircons exhibit patterns that are comparable to those of Upper Permian-Middle Triassic turbidites of the Youjiang region (Fig. 12; Yang et al., 2012a, 2012b). In Th/U vs. Nb/Hf and Th/Nb vs. Hf/Th plots (Fig. 13; Yang et al., 2014), Xiaomei detrital zircons fall predominantly in the arc-related/orogenic zone, matching well with those of Upper Permian to Middle Triassic clastic rocks regionally. The 420–480 Ma peak was caused by a tectonic switch from a source in the Emeishan large igneous province (ELIP) to an Indosinian orogenic source during the Late Permian to Middle Triassic (Yang et al., 2014) (Fig. 12G–I). Upper Permian sandstone and mudstone primarily originated from weathering of ELIP basalts in the northwestern part of the Youjiang Basin (He et al., 2007), whereas Lower-Middle Triassic clastic rocks mainly originated from erosion of the Neo-Indosinian Orogen in the western part of the basin as well as Lower Paleozoic sandstones in the middle-southeastern part of the South China Craton (Wang et al., 2007a, 2007b, 2011; Li et al., 2011; Xu et al., 2011) (Fig. 1C).

The zircon age distribution in Sample BSXM-3 of the Xiaomei profile is slightly different from those of Samples BSXM-1 and -2. The former sample exhibits zircon ages concentrated at 240–280 Ma (peak ~260 Ma), 420–480 Ma (peak ~440 Ma), and 900–1000 Ma, whereas the latter two samples show a much stronger ~440-Ma peak. This suggests that Samples BSXM-1 and -2 may also have been influenced by mixing of weathered materials from the South China Craton as a result of erosion during Early to early Middle Pleistocene time (Fig. 1C). These observations are all supportive of the proximal provenance of the Xiaomei red earth sequence.

6. Conclusions

The Xiaomei red earth deposits are composed mainly of quartz and the clay minerals kaolinite, illite and mixed-layer illite/vermiculite with minor amounts of hematite and goethite. The major- and trace-element compositions exhibit pronounced differences from those of CLP loess-paleosols, UCC and PAAS. Specifically, the Xiaomei red earth deposits differ from the loess-paleosols of northern China in having lower $\varepsilon_{Nd}(0)$ values and more uniform $^{147}Sm/^{144}Nd$, $^{143}Nd/^{144}Nd$, $^{87}Sr/^{86}Sr$, and Rb/Sr ratios. Instead, the Xiaomei red earth is similar to other Upper Quaternary red earth deposits in southern China that have undergone intensive chemical weathering, including those at Xuancheng and Jiujiang on the middle to lower reaches of the Yangtze River basin. The relatively uniform La/Th ratios and REE distributions indicate that the Xiaomei red earth sediments experienced strong mixing prior to deposition, consistent with their mainly fluvial origin.

U-Pb dating of detrital zircons from the Xiaomei red earth sequence yielded consistent and stable age groups, with peaks at 240–300, 420–480, and 900–1000 Ma. This pattern is unlike those of northern Chinese loess-paleosols and their source regions. On the other hand, the age distributions for zircons from the lower Xiaomei section match well with those of Upper Permian-Middle Triassic siliciclastic rocks in the Youjiang area, and those of the middle and upper Xiaomei section show the same pattern with additional influences of zircons sourced from the South China Craton. These observations suggest that the Xiaomei red earth sediments originated mainly through weathering of Upper Permian-Middle Triassic siliciclastic rocks in the Youjiang Basin and from the South China Craton as a result of neotectonic uplift during Early Pleistocene to early Middle Pleistocene time. The generally proximal origin of the Xiaomei red earth sediments implies that the carrying capacity of the East Asian winter monsoon has been overestimated in previous provenance studies of southern Chinese red earth deposits.

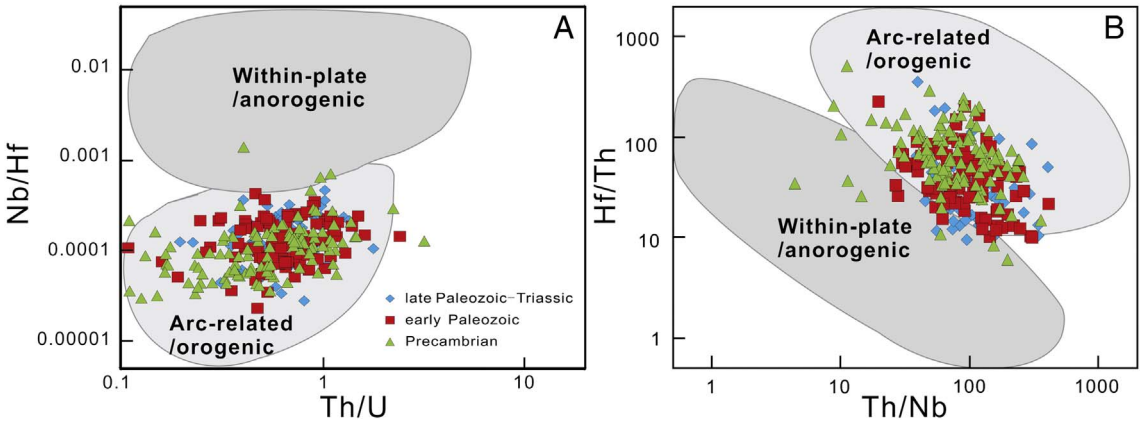

Fig. 14. (A) Th/U vs. Nb/Hf, and (B) Th/Nb vs. Hf/Th discriminant plots for zircons in Xiaomei red earth sediments.

Supplementary data to this article can be found online at https://doi.org/10.1016/j.palaeo.2017.08.040.

Acknowledgments

We hereby give our thanks to Mao Q.X., Zhao Y. and Li Y. for their participation in field work, Dr. Zheng H.T. for XRF measurements, Prof. Zhou L. for isotope measurements, and Prof. Hu Z.C. for LA-ICP-MS measurements. The authors are grateful for the assistance of Liu Z., Chen J.J., Cao S.Q. and Ye H. in LA-ICP-MS measurements and for assistance of Zhou P. and Li C.R. in data analysis. This work was supported by National Natural Science Foundation of China (Projects 41472041, 41772032, 41402036, and 41602037). C.J. Bae acknowledges financial support from the Wenner-Gren Foundation (Grant #9139) for his research in China.

References

An, Z. (Ed.), 2014. Late Cenozoic Climate Change in Asia: Loess, Monsoon and Monsoon-arid Environment Evolution. vol. 16 Springer Science & Business Media.
Andersen, T., 2002. Correction of common lead in U-Pb analyses that do not report ^{204}Pb. Chem. Geol. 192 (1), 59–79.
Andersen, T., 2005. Detrital zircons as tracers of sedimentary provenance: limiting conditions from statistics and numerical simulation. Chem. Geol. 216 (3), 249–270.
Belousova, E.A., Griffin, W.L., Pearson, N.J., 1998. Trace element composition and cathodoluminescence properties of southern African kimberlitic zircons. Mineral. Mag. 62 (3), 355–366.
Belousova, E.A., Griffin, W.L., O'Reilly, S.Y., Fisher, N.I., 2002. Igneous zircon: trace element composition as an indicator of source rock type. Contrib. Mineral. Petrol. 143 (5), 602–622.
Blum, J.D., Erel, Y., Brown, K., 1993. ^{87}Sr/^{86}Sr ratios of Sierra Nevada stream waters: implications for relative mineral weathering rates. Geochim. Cosmochim. Acta 57 (21), 5019–5025.
Bookhagen, B., Thiede, R.C., Strecker, M.R., 2005. Late Quaternary intensified monsoon phases control landscape evolution in the northwest Himalaya. Geology 33 (2), 149–152.
Boulay, S., Colin, C., Trentesaux, A., Frank, N., Liu, Z., 2005. Sediment sources and East Asian monsoon intensity over the last 450 ky. Mineralogical and geochemical investigations on South China Sea sediments. Palaeogeogr. Palaeoclimatol. Palaeoecol. 228 (3-4), 260–277.
Bronger, A., Heinkele, T., 1990. Mineralogical and clay mineralogical aspects of loess research. Quat. Int. 7, 37–51.
Che, X., Li, G., 2013. Binary sources of loess on the Chinese Loess Plateau revealed by U-Pb ages of zircon. Quat. Res. 80 (3), 545–551.
Corfu, F., Hanchar, J.M., Hoskin, P.W., Kinny, P., 2003. Atlas of zircon textures. Rev. Mineral. Geochem. 53 (1), 469–500.
Costantini, E.A.C., Makeev, A., Sauer, D., 2009. Recent developments and new frontiers in paleopedology. Quat. Int. 209 (1), 1–5.
Derbyshire, E., Meng, X., Kemp, R.A., 1998. Provenance, transport and characteristics of modern aeolian dust in western Gansu Province, China, and interpretation of the Quaternary loess record. J. Arid Environ. 39 (3), 497–516.
Ding, Z., Sun, J., Yang, S., Liu, T., 2001. Geochemistry of the Pliocene red clay formation in the Chinese Loess Plateau and implications for its origin, source provenance and paleoclimate change. Geochim. Cosmochim. Acta 65 (6), 901–913.
Ding, Z., Derbyshire, E., Yang, S., Yu, Z., Xiong, S., Liu, T., 2002. Stacked 2.6-Ma grain size record from the Chinese loess based on five sections and correlation with the deep-sea δ^{18}O. Paleoceanography 17 (3), 5:1–5:21.
Du, Y., Xu, Y., 2012. A preliminary study on Caledonian event in South China. Geol. Sci. Technol. Inf. 5, 007 (in Chinese with English abstract).
Gallet, S., Jahn, B., Torii, M., 1996. Geochemical characterization of the Luochuan loess-paleosol sequence, China, and paleoclimatic implications. Chem. Geol. 133 (1), 67–88.
Gallet, S., Jahn, B., Van Vliet Lanoë, B., Dia, A., Rossello, E., 1998. Loess geochemistry and its implications for particle origin and composition of the upper continental crust. Earth Planet. Sci. Lett. 156 (3–4), 157–172.
Goldstein, S.J., Jacobsen, S.B., 1987. The Nd and Sr isotopic systematics of river-water dissolved material: implications for the sources of Nd and Sr in seawater. Chem. Geol. 66 (3), 245–272.
Goldstein, S.L., O'Nions, R.K., Hamilton, P.J., 1984. A Sm-Nd isotopic study of atmospheric dusts and particulates from major river systems. Earth Planet. Sci. Lett. 70 (2), 221–236.
Hanchar, J., Van, W.W., 2007. Rare earth element behavior in zircon-melt systems. Elements 3 (1), 37–42.
Hao, Q., Guo, Z., Qiao, Y., Xu, B., Oldfield, F., 2010. Geochemical evidence for the provenance of middle Pleistocene loess deposits in southern China. Quat. Sci. Rev. 29 (23–24), 3317–3326.
He, B., Xu, Y., Huang, X., Luo, Z., Shi, Y., Yang, Q., Yu, S., 2007. Age and duration of the Emeishan flood volcanism, SW China: geochemistry and SHRIMP zircon U-Pb dating of silicic ignimbrites, post-volcanic Xuanwei Formation and clay tuff at the Chaotian section. Earth Planet. Sci. Lett. 255 (3–4), 306–323.
Holland, H.D., 1978. The Chemistry of the Atmosphere and Oceans. John Wiley & Sons, New York (351 pp).
Hong, H., Gu, Y., Li, R., Zhang, K., Li, Z., 2010. Clay mineralogy and geochemistry and their palaeoclimatic interpretation of the Pleistocene deposits in the Xuancheng section, southern China. J. Quat. Sci. 25 (5), 662–674.
Hong, H., Wang, C., Zeng, K., Gu, Y., Wu, Y., Yin, K., Li, Z., 2013. Geochemical constraints on provenance of the mid-Pleistocene red earth sediments in subtropical China. Sediment. Geol. 290, 97–108.
Hoskin, P.W.O., Ireland, T.R., 2000. Rare earth element chemistry of zircon and its use as a provenance indicator. Geology 28 (7), 627–630.
Hoskin, P.W., Schaltegger, U., 2003. The composition of zircon and igneous and metamorphic petrogenesis. Rev. Mineral. Geochem. 53 (1), 27–62.
Hou, Y., Richard, P., Yuan, B., Guo, Z., Alan, D., Wang, W., Jennifer, C., Xie, G., Huang, W., 2000. Mid-Pleistocene Acheulean-like stone technology of the Bose basin, South China. Science 287 (5458), 1622–1626.
Hu, X., Cheng, T., Wu, H., 2003. Do multiple cycles of aeolian deposit-pedogenesis exist in the reticulate red clay sections in southern China? Chin. Sci. Bull. 48 (12), 1251–1258.
Hu, X., Zhu, Y., Shen, M., 2005. Grain-size evidence for multiple origins of the reticulate red clay in southern China. Chin. Sci. Bull. 50 (09), 910–918.
Jackson, S.E., Pearson, N.J., Griffin, W.L., Belousova, E.A., 2004. The application of laser ablation-inductively coupled plasma-mass spectrometry to in situ U-Pb zircon geochronology. Chem. Geol. 211 (1), 47–69.
Jahn, B., Condie, K.C., 1995. Evolution of the Kaapvaal Craton as viewed from geochemical and Sm-Nd isotopic analyses of intracratonic pelites. Geochim. Cosmochim. Acta 59 (11), 2239–2258.
Jahn, B., Gallet, S., Han, J., 2001. Geochemistry of the Xining, Xifeng and Jixian sections, Loess Plateau of China: eolian dust provenance and paleosol evolution during the last 140 ka. Chem. Geol. 178 (1), 71–94.
Jiang, H., Ding, Z., 2010. Eolian grain-size signature of the Sikouzi lacustrine sediments (Chinese Loess Plateau): implications for Neogene evolution of the East Asian winter monsoon. Geol. Soc. Am. Bull. 122 (5–6), 843–854.
Li, L., Sun, M., Wang, Y., Xing, G., Zhao, G., Lin, S., Xia, X., Chan, L., Zhang, F., Wong, J., 2011. U-Pb and Hf isotopic study of zircons from migmatised amphibolites in the Cathaysia Block: implications for the early Paleozoic peak tectonothermal event in Southeastern China. Gondwana Res. 19 (1), 191–201.
Liu, Y., Zong, K., Kelemen, P.B., Gao, S., 2008a. Geochemistry and magmatic history of eclogites and ultramafic rocks from the Chinese continental scientific drill hole: subduction and ultrahigh-pressure metamorphism of lower crustal cumulates. Chem. Geol. 247 (1), 133–153.
Liu, Y., Hu, Z., Gao, S., Günther, D., Xu, J., Gao, C., Chen, H., 2008b. In situ analysis of major and trace elements of anhydrous minerals by LA-ICP-MS without applying an internal standard. Chem. Geol. 257 (1), 34–43.
Liu, Y., Gao, S., Hu, Z., Gao, C., Zong, K., Wang, D., 2010. Continental and oceanic crust recycling-induced melt-peridotite interactions in the Trans-North China Orogen: U-Pb dating, Hf isotopes and trace elements in zircons from mantle xenoliths. J. Petrol. 51 (1–2), 537–571.
Liu, F., Li, G., Chen, J., 2014. U-Pb ages of zircon grains reveal a proximal dust source of the Xiashu loess, Lower Yangtze River region, China. Chin. Sci. Bull. 59 (20), 2391–2395.
Ludwig, K.R., 2006. Isoplot/Ex version 3.41 d: a geochronological toolkit for Microsoft Excel. In: Berkeley Geochronology Center: Special Publication 4.
McLennan, S.M., 1989. Rare earth elements in sedimentary rocks; influence of provenance and sedimentary processes. Rev. Mineral. Geochem. 21 (1), 169–200.
Nesbitt, H.W., Young, G.M., 1982. Early Proterozoic climates and plate motions inferred from major element chemistry of lutites. Nature 299 (5885), 715–717.
Pullen, A., Kapp, P., McCallister, A.T., Chang, H., Gehrels, G.E., Garzione, C.N., Heermance, R.V., Ding, L., 2011. Qaidam Basin and northern Tibetan Plateau as dust sources for the Chinese Loess Plateau and paleoclimatic implications. Geology 39 (11), 1031–1034.
Qiao, Y., Hao, Q., Peng, S., Wang, Y., Li, J., Liu, Z., 2011. Geochemical characteristics of the eolian deposits in southern China, and their implications for provenance and weathering intensity. Palaeogeogr. Palaeoclimatol. Palaeoecol. 308 (3–4), 513–523.
Rubatto, D., Gebauer, D., 2000. Use of cathodoluminescence for U-Pb zircon dating by ion microprobe: some examples from the Western Alps. In: Pagel, M., Barbin, V., Blanc, P., Ohnenstetter, D. (Eds.), Cathodoluminescence in Geosciences. Springer, Berlin, pp. 373–400.
Sheldon, N.D., Tabor, N.J., 2009. Quantitative paleoenvironmental and paleoclimatic reconstruction using paleosols. Earth Sci. Rev. 95 (1), 1–52.
Stevens, T., Palk, C., Carter, A., Lu, H., Clift, P.D., 2010. Assessing the provenance of loess and desert sediments in northern China using U-Pb dating and morphology of detrital zircons. Geol. Soc. Am. Bull. 122 (7–8), 1331–1344.
Sun, W., McDonough, F.W., 1989. Chemical and isotopic systematics of oceanic basalts: implications for mantle composition and processes. In: Saunders, D., Norry, M.J. (Eds.), Magmatism in the Ocean Basins. Geological Society of London, Special Publication 42pp. 313–345.
Taylor, S.R., McLennan, S.M., 1985. The Continental Crust: Its Composition and Evolution. Blackwell, Oxford (312 pp).
Újvári, G., Varga, A., Ramos, F.C., Kovács, J., Németh, T., Stevens, T., 2012. Evaluating the use of clay mineralogy, Sr-Nd isotopes and zircon U-Pb ages in tracking dust provenance: an example from loess of the Carpathian Basin. Chem. Geol. 304-305, 83–96.
Wang, W., Bae, C.J., 2015. How old are the Bose (Baise) Basin (Guangxi, southern China) bifaces? The Australasian tektites question revisited. J. Hum. Evol. 80, 171–174.
Wang, Y., Fan, W., Sun, M., Liang, X., Zhang, Y., Peng, T., 2007a. Geochronological, geochemical and geothermal constraints on petrogenesis of the Indosinian

peraluminous granites in the South China Block: a case study in the Hunan Province. Lithos 96 (3–4), 475–502.
Wang, Y., Fan, W., Cawood, P.A., Ji, S., Peng, T., Chen, X., 2007b. Indosinian high-strain deformation for the Yunkaidashan tectonic belt, south China: kinematics and $^{40}Ar/^{39}Ar$ geochronological constraints. Tectonics 26 (6), 1–21.
Wang, A., Smith, J.A., Wang, G., Zhang, K., Xiang, S., Liu, D., 2009. Late Quaternary river terrace sequences in the eastern Kunlun Range, northern Tibet: a combined record of climatic change and surface uplift. J. Asian Earth Sci. 34 (4), 532–543.
Wang, Y., Zhang, A., Fan, W., Zhao, G., Zhang, G., Zhang, Y., Zhang, F., Li, S., 2011. Kwangsian crustal anatexis within the eastern South China Block: geochemical, zircon U-Pb geochronological and Hf isotopic fingerprints from the gneissoid granites of Wugong and Wuyi-Yunkai Domains. Lithos 127 (1–2), 239–260.
Wang, L., Yu, J., Griffin, W.L., O Reilly, S.Y., 2012. Early crustal evolution in the western Yangtze Block: evidence from U-Pb and Lu-Hf isotopes on detrital zircons from sedimentary rocks. Precambrian Res. 222, 368–385.
Weldeab, S., Emeis, K., Hemleben, C., Siebel, W., 2002. Provenance of lithogenic surface sediments and pathways of riverine suspended matter in the Eastern Mediterranean Sea: evidence from $^{143}Nd/^{144}Nd$ and $^{87}Sr/^{86}Sr$ ratios. Chem. Geol. 186 (1), 139–149.
Wiedenbeck, M., Alle, P., Corfu, F., Griffin, W.L., Meier, M., Von Quadt, A., Roddick, J.C., 1995. Three natural zircons standards for U-Th-Pb, Lu-Hf, trace element and REE analyses. Geostand. Geoanal. Res. 19 (1), 1–23.
Xiao, G., Zong, K., Li, G., Hu, Z., Dupont Nivet, G., Peng, S., Zhang, K., 2012. Spatial and glacial-interglacial variations in provenance of the Chinese Loess Plateau. Geophys. Res. Lett. 39 (20), 6.
Xie, J., Yang, S., Ding, Z., 2012. Methods and application of using detrital zircons to trace the provenance of loess. Sci. China D Earth Sci. 55 (11), 1837–1846.
Xiong, S., Sun, D., Ding, Z., 2002. Aeolian origin of the red earth in southeast China. J. Quat. Sci. 17 (2), 181–191.
Xu, X., Zhang, Y., Shu, L., Jia, D., 2011. La-ICP-MS U-Pb and $^{40}Ar/^{39}Ar$ geochronology of the sheared metamorphic rocks in the Wuyishan: constraints on the timing of Early Paleozoic and Early Mesozoic tectono-thermal events in SE China. Tectonophysics 501 (1–4), 71–86.
Yang, S., Li, C., Yang, D., Li, X., 2004. Chemical weathering of the loess deposits in the lower Changjiang Valley, China, and paleoclimatic implications. Quat. Int. 117 (1), 27–34.
Yang, J., Cawood, P.A., Du, Y., Huang, H., Hu, L., 2012a. Detrital record of Indosinian mountain building in SW China: provenance of the Middle Triassic turbidites in the Youjiang Basin. Tectonophysics 574-575, 105–117.
Yang, J., Cawood, P.A., Du, Y., Huang, H., Huang, H., Tao, P., 2012b. Large Igneous Province and magmatic arc sourced Permian-Triassic volcanogenic sediments in China. Sediment. Geol. 261-262, 120–131.
Yang, J., Cawood, P.A., Du, Y., Huang, H., Hu, L., 2014. A sedimentary archive of tectonic switching from Emeishan Plume to Indosinian orogenic sources in SW China. J. Geol. Soc. Lond. 171 (2), 269–280.
Yao, J., Shu, L., Santosh, M., 2011. Detrital zircon U-Pb geochronology, Hf-isotopes and geochemistry—new clues for the Precambrian crustal evolution of Cathaysia Block, South China. Gondwana Res. 20 (2–3), 553–567.
Ye, W., Yang, L., Zhu, L., Li, F., Wang, J., 2008. Characteristics and origin of rare earth elements of vermicular red earth in middle sub-tropic zone. Sci. Geogr. Sin. 28 (1), 40–44 (in Chinese with English abstract).
Yuan, B., Xia, Z., Li, B., Qiao, Y., Gu, Z., Zhang, J., Xu, B., Huang, W., Zeng, R., 2008. Chronostratigraphy and stratigraphic division of red soil in southern China. Quat. Sci. 28 (1), 1–12 (in Chinese with English abstract).
Zhang, Q., Zhu, C., Jiang, T., Becker, S., 2005. Mid-Pleistocene environmental reconstruction based on Xiashu loess deposits in the Yangtze Delta, China. Quat. Int. 135 (1), 131–137.